Electronic Supplementary Material (ESI) for Journal of Materials Chemistry C.

Supplementary information

Pyrolyzed Chitin Nanofiber Paper as a Three-Dimensional Porous and Defective Nanocarbon for Photosensing and Energy Storage

Luting Zhu, Yintong Huang, Yoshitaka Morishita, Kojiro Uetani, Masaya Nogi, Hirotaka Koga*

The Institute of Scientific and Industrial Research, Osaka University, 8-1 Mihogaoka, Ibaraki, Osaka 567-0047, Japan

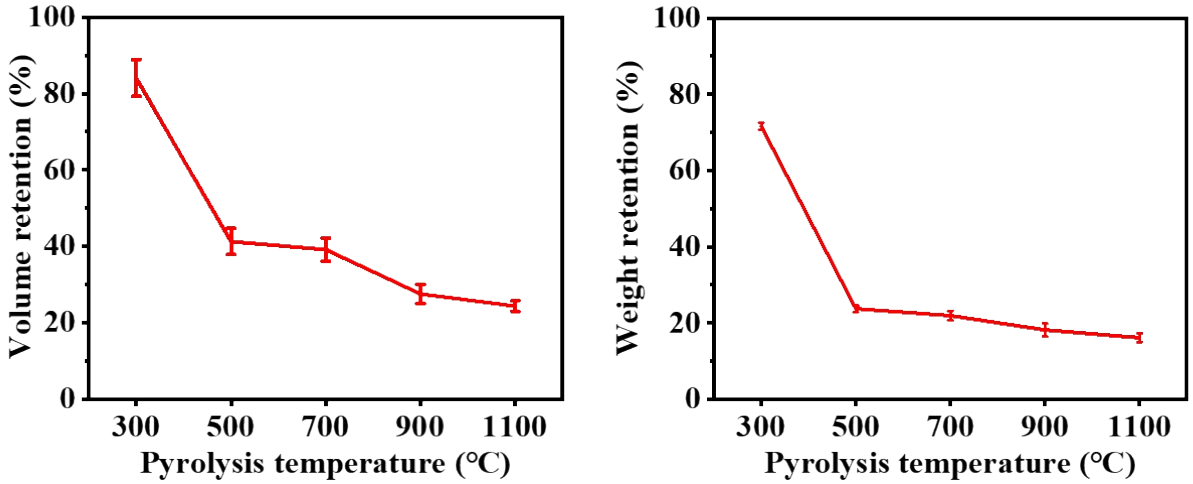

Figure S1. Volume and weight retention of the chitin nanofiber papers pyrolyzed at different temperatures.

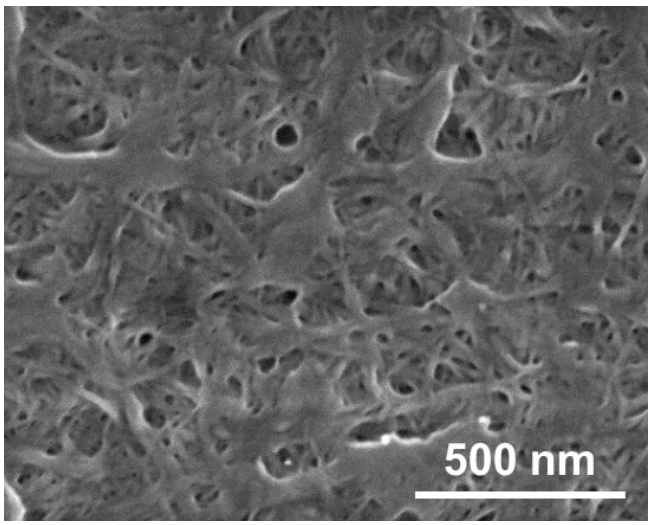

Figure S2. FE-SEM image of the chitin nanofiber paper prepared without *t*-butyl alcohol treatment by freeze drying.

The chitin nanofiber paper prepared without *t*-butyl alcohol by freeze drying had densely packed structures, which were derived from aggregation of the nanofibers owing to drying in the presence of water with high surface tension.

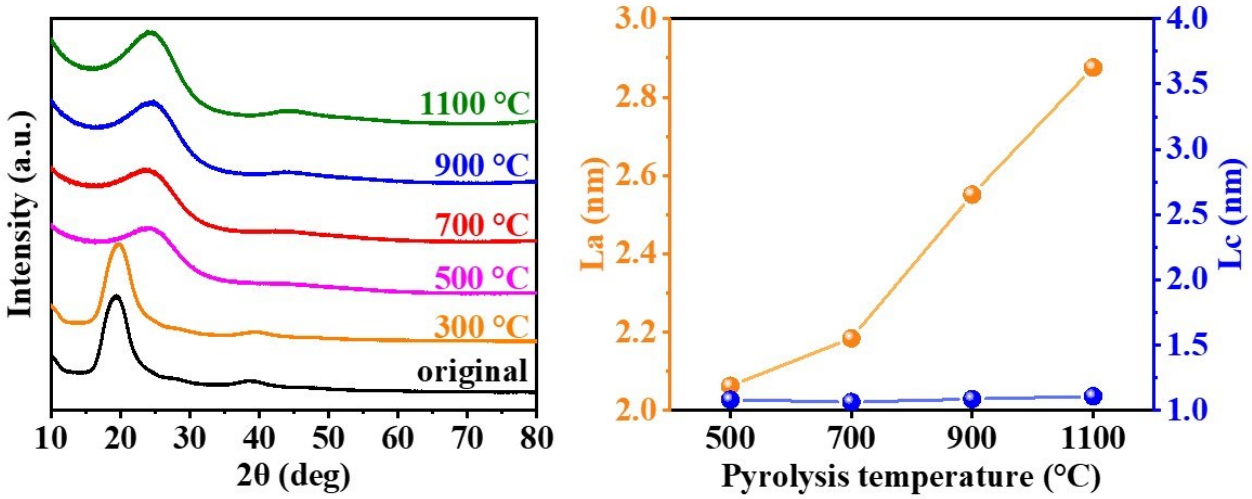

Figure S3. XRD spectra (left) and crystallite sizes of the graphene fragment in in-plane (L_a) and stacking (L_c) direction (right) for the chitin nanofiber paper pyrolyzed at different temperatures.

The crystal structure of chitin disappeared after pyrolysis at above 500 °C. The XRD peaks at 2θ = ca. 22° and 44°, which were derived from the (002) and (10) crystal planes of graphite, respectively,[1] appeared for pyrolysis above 500 °C, suggesting that graphitic carbon structures formed. To estimate the growth of the graphitic carbon structures (graphitic sp^2-hybridized carbon domains) upon pyrolysis, their crystallite sizes in in-plane (L_a) and stacking (L_c) direction were calculated; L_a and L_c were calculated from the (10) and (002) reflection of graphite at 2θ= ca. 44° (interplanar distance d_a= ca. 0.2 nm) and 22° (d_c= ca. 0.4 nm), respectively, using a Scherrer's formula.[1,2] Then, the graphitic sp^2-hybridized carbon domains increased their average width (L_a) from ca. 2.0 to ca. 2.9 nm, while their average thickness (L_c) was kept almost constant at ca. 1.2 nm. This result indicated that the graphitic carbon structures were gradually grown in the in-plane direction upon pyrolysis of the chitin nanofiber papers.

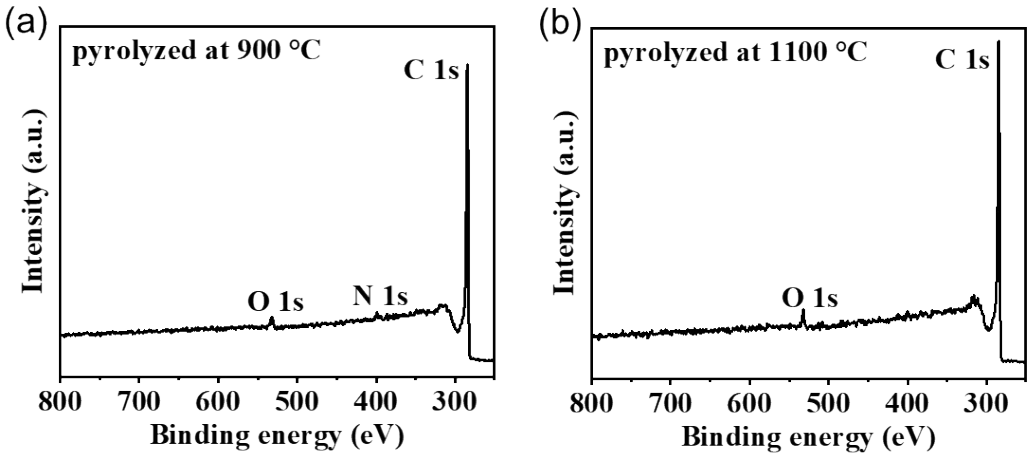

Figure S4. Wide XPS spectra of the chitin nanofiber papers pyrolyzed at (a) 900 and (b) 1100 °C.

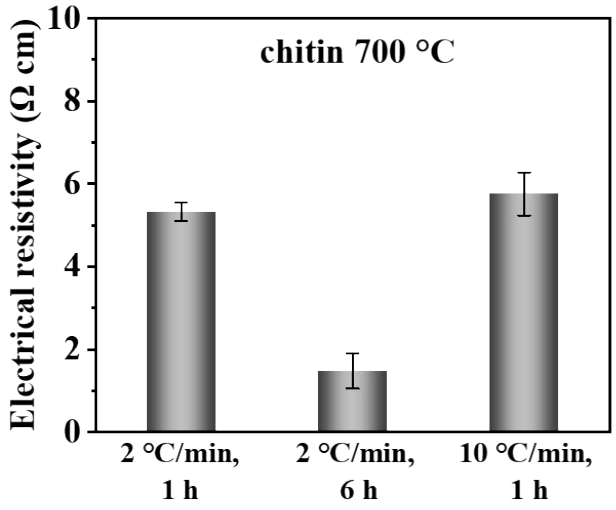

Figure S5. Effect of the pyrolysis time and the heating/cooling speed on the electrical resistivity of the chitin nanofiber paper pyrolyzed at 700 °C.

When the pyrolysis time was extended from 1 to 6 h at a heating/cooling speed of 2 °C min^{-1}, the electrical resistivity of the resulting pyrolyzed chitin nanofiber paper was decreased from ca. 5.3 to ca. 1.5 Ω cm. When the heating/cooling speed was increased from 2 to 10 °C min^{-1} at a pyrolysis time of 1 h, the electrical resistivity of the resulting pyrolyzed chitin nanofiber paper was slightly increased from ca. 5.3 to ca. 5.8 Ω cm. These results suggested that the pyrolysis time and the heating/cooling speed can also tune the electrical resistivity of the pyrolyzed chitin nanofiber paper, while the pyrolysis temperature would be more dominant (see also Figure 4).

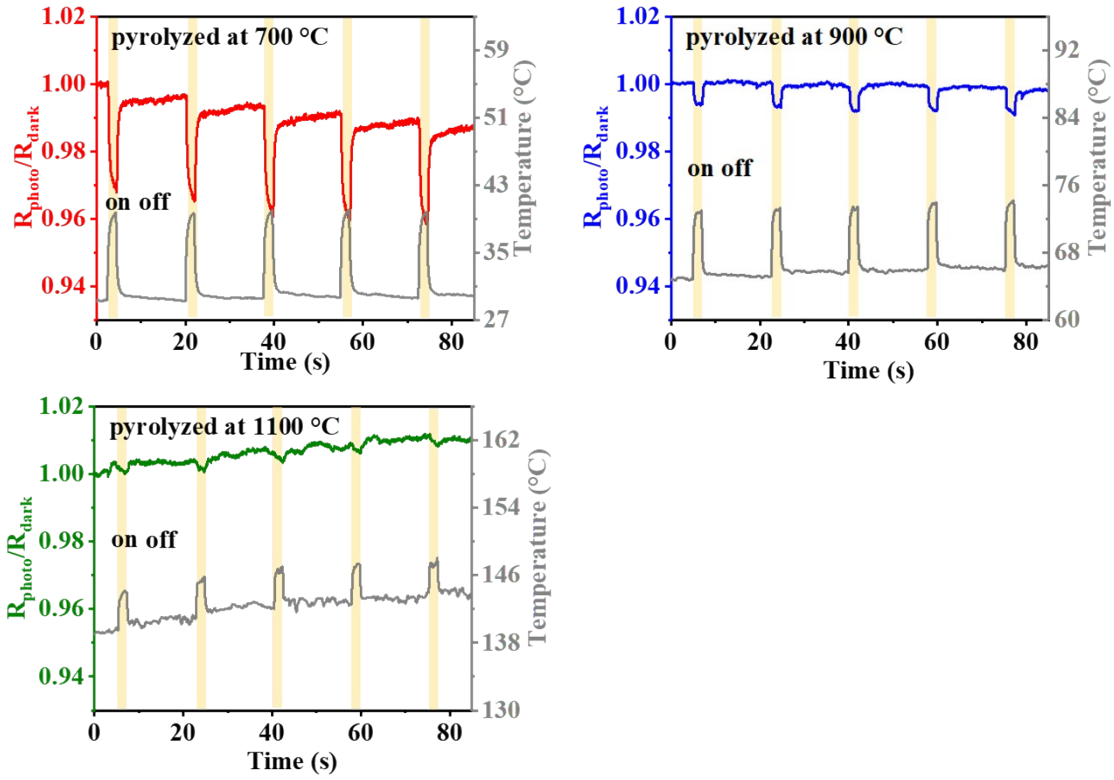

Figure S6. Change in the electrical resistance and surface temperature upon exposure to solar light for the chitin nanofiber papers pyrolyzed at different temperatures. Light intensity 1 sun, irradiation time 2 s, and applied voltage 5 V.

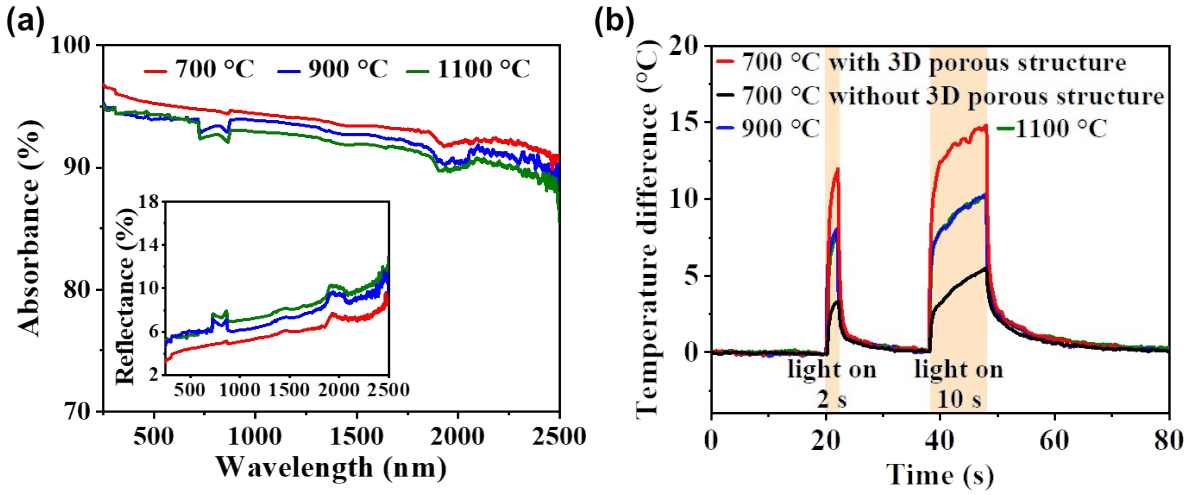

Figure S7. (a) UV–vis–NIR absorption spectra of the chitin nanofiber papers with 3D porous structures at different pyrolysis temperatures, and (b) change in the surface temperature upon exposure to solar light for the chitin nanofiber papers with and without 3D porous structures pyrolyzed at 700 °C, and those with 3D porous structures pyrolyzed at 900 and 1100 °C. Light intensity 1 sun, irradiation time 2 or 10 s, no applied voltage.

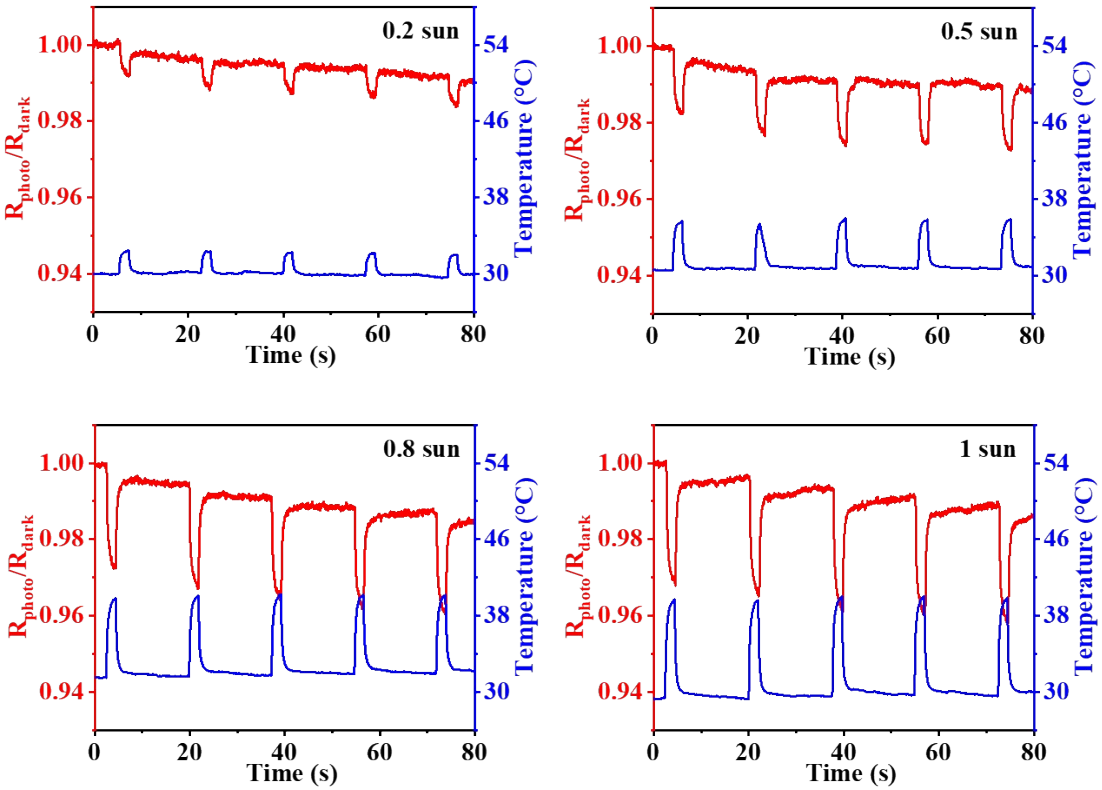

Figure S8. Change in the electrical resistance and surface temperature upon exposure to solar light at different intensities for the chitin nanofiber paper pyrolyzed at 700 °C with 3D porous structures. Irradiation time 2 s.

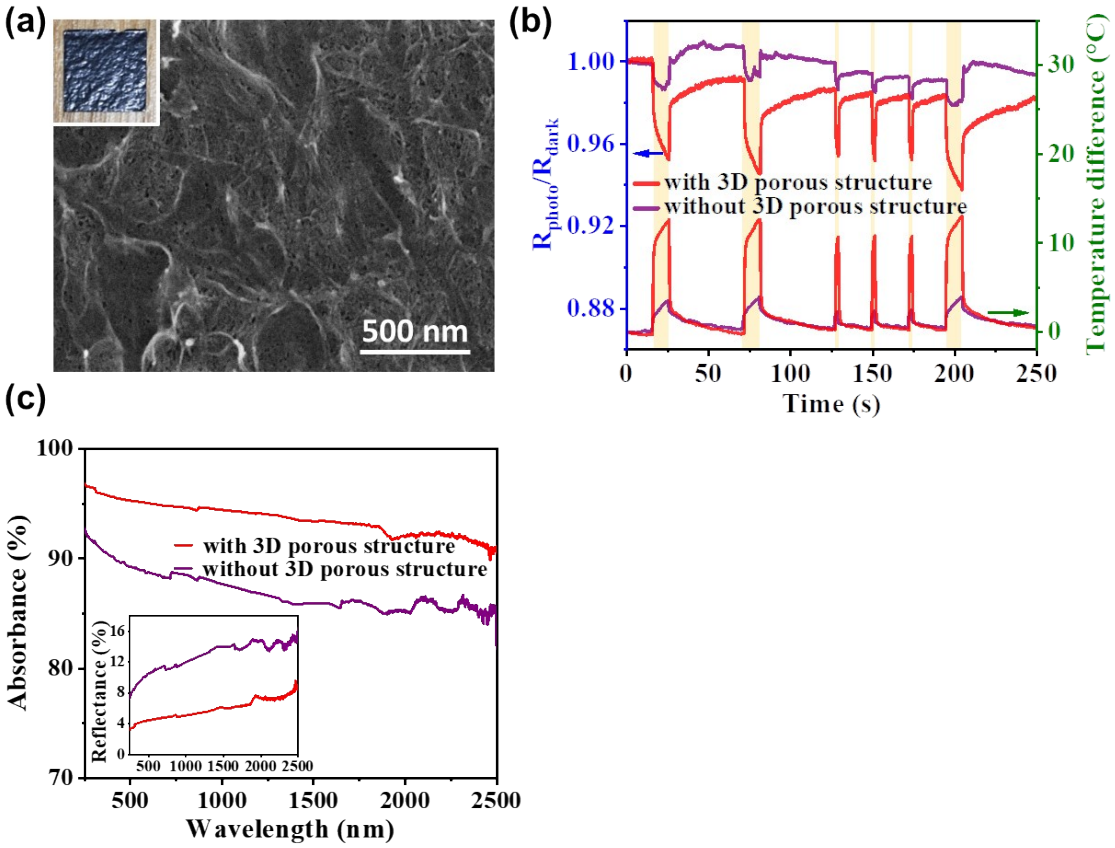

Figure S9. (a) Optical (insert) and FE-SEM images of the chitin nanofiber paper without 3D porous structures pyrolyzed at 700 °C. (b) Change in the electrical resistance and surface temperature, and (c) UV–vis–NIR absorption spectra of the chitin nanofiber papers with and without 3D porous structures pyrolyzed at 700 °C.

The chitin nanofiber paper without 3D porous structures was prepared without t-butyl alcohol treatment and by hot-press drying at 1 MPa and 110 °C for 20 min, instead of freeze drying, followed by pyrolysis at 700 °C (Fig. S9a). The pyrolyzed chitin nanofiber paper without 3D porous nanostructures showed inferior sensitivity to that with 3D porous nanostructures (Figure S9b). The poor sensitivity was because of its lower temperature increase, which is ascribed to the higher reflectance and lower absorbance of the pyrolyzed chitin nanofiber paper without 3D porous nanostructures than that with 3D porous nanostructures (Figure S9c). In other words, the 3D porous structures promoted solar light absorption and thus photothermal heating, enhancing the photosensing performance.

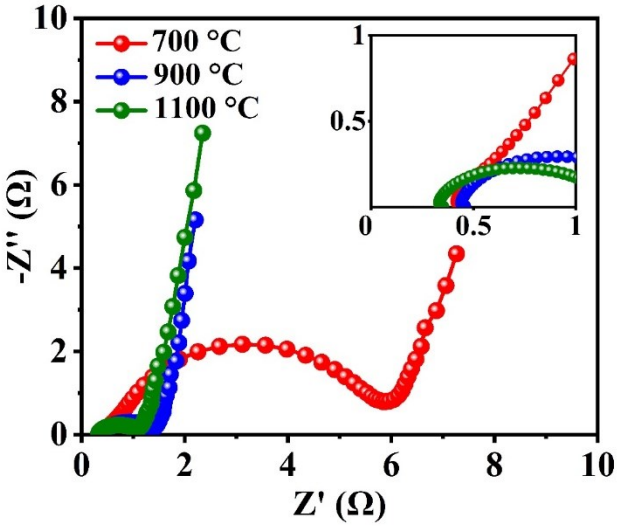

Figure S10. Nyquist plots of the pyrolyzed chitin nanofiber papers.

The Nyquist plots consisted of a semicircle in the high-frequency region and a linear line in the low-frequency region.[3] The low intercept of the semicircle with the real axis refers to the low intrinsic resistance of the electrolyte (R_s). The diameter of the semicircle refers to the interfacial charge-transfer resistance at the electrode–electrolyte interface (R_{ct}), which is related to the electrical conductivity of the electrode. A more vertical line in the low frequency region represents lower ionic diffusion resistance in the electrode materials. Therefore, the chitin nanofiber paper pyrolyzed at 700 °C showed higher interfacial charge-transfer resistance and ionic diffusion resistance in the electrode than the chitin nanofiber papers pyrolyzed at 900 and 1100 °C.

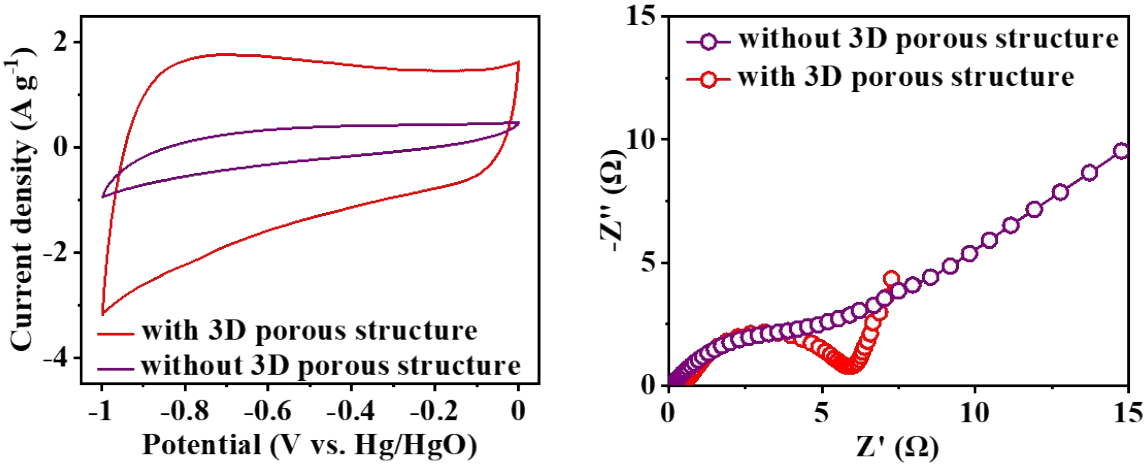

Figure S11. Cyclic voltammetry curves at a scan rate of 10 mV s^{-1} and Nyquist plots of the chitin nanofiber papers with and without 3D porous structures pyrolyzed at 700 °C.

The pyrolyzed chitin nanofiber paper with 3D porous structures had a more vertical line in the low frequency region, representing lower ionic diffusion resistance because of the 3D interconnected network.

Table S1. Specific capacitance values of biomass-derived nanocarbon materials

Materials	Surface area (m^2 g^{-1})	N %	Additive in electrode	Electrolyte	Capacitance (F g^{-1})	Ref.
Pyrolyzed chitin nanofiber paper	719	5.74	no	6 M KOH	208 (0.5 A g^{-1}) 184 (1 A g^{-1})	This work
Chitin nanogel-derived N-doped carbon nanospheres	1031	3.2	acetylene black & binder	1 M H_2SO_4	192 (0.5 A g^{-1})	4
Cellulose nanocrystal/ cellulose nanofibril-derived carbon film	1244	0	carbon black & binder	2 M KOH	170 (0.5 A g^{-1})	5
Cellulose-derived N-doped carbon	472	3.61	no	1 M H_2SO_4	193 (0.5 A g^{-1})	6
Cotton-derived N-doped carbon	617	9.0	carbon black & binder	6 M KOH	180 (0.5 A g^{-1})	7
Lignin-derived hierarchical porous carbon	907	-	carbon black & binder	1 M H_2SO_4	168 (10 mV s^{-1})	8
Starch-derived porous carbon	1239	0	carbon black & binder	6 M KOH	144 (0.625 A g^{-1})	9
Alginate-derived porous carbon	704	0	acetylene black & binder	6 M KOH	183 (0.5 A g^{-1})	10

Note: The specific capacitance values shown in this Table were calculated in three-electrode systems.

References

1 K. Tanaka, M. Ueda, T. Koike, T. Yamabe and S. Yata, *Synth. Met.*, 1988, **25**, 265–275.

2 J. Biscoe and B. E. Warren, *J. Appl. Phys.*, 1942, **13**, 364–371.

3 L. Gao, L. Xiong, D. Xu, J. Cai, L. Huang, J. Zhou and L. Zhang, *ACS Appl. Mater. Interfaces*, 2018, **10**, 28918–28927.

4 S. Zheng, Y. Cui, J. Zhang, Y. Gu, X. Shi, C. Peng and D. Wang, *RSC Adv.*, 2019, **9**, 10976–10982.

5 Z. Li, K. Ahadi, K. Jiang, B. Ahvazi, P. Li, A. O. Anyia, K. Cadien and T. Thundat, *Nano Res.*, 2017, **10**, 1847–1860.

6 Z. Chen, X. Peng, X. Zhang, S. Jing, L. Zhong and R. Sun, *Carbohydr. Polym.*, 2017, **170**, 107–116.

7 L. Chen, T. Ji, L. Mu and J. Zhu, *Carbon*, 2017, **111**, 839–848.

8 W. Zhang, H. Lin, Z. Lin, J. Yin, H. Lu, D. Liu and M. Zhao, *ChemSusChem*, 2015, **8**, 2114–2122.

9 L. Pang, B. Zou, Y. Zou, X. Han, L. Cao, W. Wang and Y. Guo, *Colloids Surfaces A Physicochem. Eng. Asp.*, 2016, **504**, 26–33.

10 W. Chen, M. Luo, K. Yang and X. Zhou, *Int. J. Biol. Macromol.*, 2020, **158**, 265–274.